

Black Holes and WIMPs: All or Nothing or Something Else

Bernard Carr,^{1,2*} Florian Kühnel,^{3†} and Luca Visinelli^{4,5‡}

¹*School of Physics and Astronomy, Queen Mary University of London, Mile End Road, London E1 4NS, UK*

²*Research Center for the Early Universe, University of Tokyo, Tokyo 113-0033, Japan*

³*Arnold Sommerfeld Center, Ludwig-Maximilians-Universität, Theresienstraße 37, 80333 München, Germany*

⁴*Gravitation Astroparticle Physics Amsterdam (GRAPPA), Institute for Theoretical Physics Amsterdam and Delta Institute for Theoretical Physics, University of Amsterdam, Science Park 904, 1098 XH Amsterdam, The Netherlands*

⁵*INFN, Laboratori Nazionali di Frascati, C.P. 13, 100044 Frascati, Italy*

Accepted XXX. Received YYY; in original form ZZZ

ABSTRACT

We consider constraints on primordial black holes (PBHs) in the mass range $(10^{-18}\text{--}10^{15}) M_\odot$ if the dark matter (DM) comprises weakly interacting massive particles (WIMPs) which form halos around them and generate γ -rays by annihilations. The observed extragalactic γ -ray background then implies that the PBH DM fraction is $f_{\text{PBH}} \lesssim 2 \times 10^{-9} (m_\chi/\text{TeV})^{1.1}$ in the mass range $2 \times 10^{-12} M_\odot (m_\chi/\text{TeV})^{-3.2} \lesssim M \lesssim 5 \times 10^{12} M_\odot (m_\chi/\text{TeV})^{1.1}$, where m_χ and M are the WIMP and PBH masses, respectively. This limit is independent of M and therefore applies for any PBH mass function. For $M \lesssim 2 \times 10^{-12} M_\odot (m_\chi/\text{TeV})^{-3.2}$, the constraint on f_{PBH} is a decreasing function of M and PBHs could still make a significant DM contribution at very low masses. We also consider constraints on WIMPs if the DM is mostly PBHs. If the merging black holes recently discovered by LIGO/Virgo are of primordial origin, this would rule out the standard WIMP DM scenario. More generally, the WIMP DM fraction cannot exceed 10^{-4} for $M > 10^{-9} M_\odot$ and $m_\chi > 10 \text{ GeV}$. There is a region of parameter space, with $M \lesssim 10^{-11} M_\odot$ and $m_\chi \lesssim 100 \text{ GeV}$, in which WIMPs and PBHs can both provide some but not all of the DM, so that one requires a third DM candidate.

Key words: black hole physics – dark matter – early Universe

1 INTRODUCTION

The recent discovery of intermediate-mass black-hole mergers by the LIGO/Virgo collaboration (Abbott et al. 2020a) has led to speculation that the dark matter (DM) might consist of black holes rather than a more conventional candidate, such as a weakly interacting massive particle (WIMP). This is due to the of the LIGO/Virgo black holes being produced through stellar collapse or multi-stage mergers. Although the LIGO/Virgo black holes might not be numerous enough to explain *all* the DM, they would need to provide at least 1% of it, which suggests the possibility of a hybrid model, in which the DM is some mixture of WIMPs and black holes.

If black holes provide more than 20% of the dark matter, the success of the cosmological nucleosynthesis scenario (Wagoner et al. 1967) implies they could not derive from baryons and would therefore need to be *primordial* in origin. The suggestion that the DM could be primordial black holes (PBHs) dates back to the 1970s (Carr & Hawking 1974; Chapline 1975) but has intensified over the past three decades, partly due to the failure to find either experimental or astronomical evidence for WIMPs. If PBHs have monochromatic mass function, there are only a few mass windows

in which they could provide all the DM but the situation is more complicated in the realistic case in which they have an extended mass function (Carr et al. 2016b). For example, one would expect the mass at which the density peaks to be less than the mass at which the LIGO/Virgo events peak, since the gravitational wave signal is stronger for more massive PBHs. In particular, it has been pointed out that the thermal history of the Universe may naturally generate a bumpy PBH mass function, which could explain the DM, the LIGO/Virgo events and various other cosmological conundra (Carr et al. 2019). For a recent comprehensive review of these issues, see Carr & Kühnel (2020).

Whether or not the black holes are primordial — and the analysis of this paper will cover both cases — there is a serious objection to hybrid models in which most of the DM comprises WIMPs. This is because they would inevitably clump in halos around the black holes, generating enhanced annihilations and γ -ray emission. As first studied by Mack et al. (2007); Ricotti (2007); Ricotti et al. (2008); Ricotti & Gould (2009); Lacki & Beacom (2010) and, more recently, by Eroshenko (2016); Boucenna et al. (2018); Eroshenko (2020); Adamek et al. (2019); Bertone et al. (2019); Cai et al. (2020), this implies very stringent constraints on hybrid scenarios, leading to the conclusion that one cannot have an

* E-mail: B.J.Carr@qmul.ac.uk

† E-mail: kuhnel@kth.se

‡ E-mail: luca.visinelli@lnf.infn.it; GRAPPA fellow & Fellini fellow

appreciable amount of DM in *both* components.¹ If nearly all the DM is WIMPs, the fraction in black holes must be tiny; but if nearly all the DM is PBHs, the fraction in WIMPs must be tiny.

However, this problem has only been investigated for a rather restricted combination of black hole and WIMP masses, so the previous analysis needs to be extended to see if this conclusion applies more generally. For example, Adamek et al. (2019) focus on the PBH mass range around $1 M_\odot$ in which the WIMP velocity distribution can be neglected but allow a range of WIMP masses (10 GeV to 1 TeV); Eroshenko (2016) focuses on the subsolar mass range where the velocity distribution must be included but assume a particular WIMP mass (70 GeV). Also we need to distinguish between the Galactic and extragalactic γ -ray backgrounds associated with WIMP annihilations, because which one dominates depends on the PBH and WIMP mass. Similar limits can be applied for Ultra-Compact Mini-Halos rather than PBHs (Scott & Sivertsson 2009; Josan & Green 2010; Bringmann et al. 2012). Note that there have also been studies of the annihilation signal from the halo of WIMPs around the supermassive black hole in the Galactic centre (Hooper & Goodenough 2011) but we do not consider this limit here.

In a companion paper (Carr et al. 2020a), we have studied *stupendously large* black holes (SLABs) in the mass range 10^{11} – $10^{18} M_\odot$. Such enormous objects might conceivably reside in galactic nuclei, since there is already evidence for black holes of up to $7 \times 10^{10} M_\odot$ (Shemmer et al. 2004) in that context. However, our considerations were mainly motivated by the apparent lack of constraints on PBHs in this mass range. Although SLABs are obviously too large to provide the DM in galactic halos, they might still have a large cosmological density. We found that the accretion constraints in this mass range are beset with astrophysical uncertainties, so the WIMP annihilation limit is the cleanest, at least if WIMPs provide most of the DM. The strongest limit then comes from the extragalactic γ -ray background and the constraint on the DM fraction is independent of the black hole mass.

At the other extreme, it is interesting to consider the possibility of stupendously *small* black holes, since there is still a window in the sub-planetary (asteroid to lunar) mass range (10^{-16} – $10^{-10} M_\odot$ or 10^{17} – 10^{23} g) where PBHs could provide the DM. Since these are much smaller $1 M_\odot$, they are necessarily primordial, so there is no longer the ambiguity associated with SLABs. The WIMP-annihilation constraints become weaker for lighter black holes, so we need to determine whether a scenario in which both WIMPs and sub-planetary PBHs have an appreciable density is necessarily excluded. If the sum of their contributions were less than 100%, one would be forced to a scenario which involves a *third* DM candidate.

To fill the gap in the previous literature, the purpose of this paper is to study the interplay between the DM candidates over the PBH mass range 10^{-18} to $10^{15} M_\odot$ and the WIMP mass range 10 GeV–1 TeV. Section 2 discusses the thermal production of WIMPs. Section 3 determines the structure of the resulting DM halos. Section 4 derives the the Galactic and extragalactic γ -ray flux from WIMP annihilations in these halos. Section 5 discusses the implications of the re-

cent LIGO/Virgo gravitational-wave events are due to merging PBHs. Section 6 concludes with a discussion of future prospects.

2 THERMAL PRODUCTION OF WIMPS

In the following, we assume that WIMPs make up their own antiparticles and that Maxwell-Boltzmann statistics suffices in describing the distribution of the particles. At temperatures much higher than the WIMP mass m_χ , the production of WIMPs in the primordial plasma of the early Universe proceeds through particle-antiparticle collisions, with rate

$$\Gamma_{\text{ann}} = \langle \sigma v \rangle_{\text{th}} n_{\text{eq}}. \quad (1)$$

Here, σ is the WIMP annihilation cross section, v is the WIMP relative velocity, angle brackets denote an average over the WIMP thermal distribution (th), and n is the WIMP number density of value n_{eq} at chemical equilibrium. In more detail, the yield $Y \equiv n/s$ in terms of the entropy density s , evolves as (Lee & Weinberg 1977; Steigman 1979)

$$\frac{dY}{dx} = \frac{1}{3H} \frac{ds}{dx} \langle \sigma v \rangle_{\text{th}} (Y^2 - Y_{\text{eq}}^2), \quad (2)$$

where $Y_{\text{eq}} \equiv n_{\text{eq}}/s$ and the independent variable $x \equiv m_\chi/T$ is inversely proportional to the plasma temperature T . This expression assumes the conservation of entropy in a comoving volume throughout its whole range of applicability. This equation can be solved numerically with the initial condition $Y = Y_{\text{eq}}$ at $x \approx 1$ to obtain the present yield Y_0 and the WIMP relic density,

$$\Omega_\chi h^2 = \frac{m_\chi s_0 Y_0 h^2}{\rho_{\text{crit}}}, \quad (3)$$

where s_0 is the entropy density at present time, $h = H_0/(100 \text{ km s}^{-1} \text{ Mpc}^{-1})$, and $\rho_{\text{crit}} = 3H_0^2/(8\pi G)$ is the present critical density in terms of Newton's constant G .

The annihilation rate governs the Boltzmann equation that tracks the number of WIMPs with time. When the annihilation rate falls below the expansion rate of the Universe at the temperature $T_F \approx m_\chi/20$, WIMP *chemical* decoupling occurs and the production of WIMPs ceases. For $T \lesssim T_F$, the number of WIMPs in a comoving volume is approximately constant to present time.

The computation of Y_0 strongly depends on the value of $\langle \sigma v \rangle_{\text{th}}$. If we can neglect co-annihilation (Griest & Seckel 1991) and Sommerfeld enhancement (Arkani-Hamed et al. 2009), we obtain (Gondolo & Gelmini 1991)

$$\langle \sigma v \rangle_{\text{th}} = \frac{\int_{4m_\chi^2}^{+\infty} ds (s - 4m_\chi^2) \sqrt{s} K_1(\sqrt{s}/T) \sigma(s)}{8m_\chi^4 T [K_2(m_\chi/T)]^2}, \quad (4)$$

where s is the center-of-mass energy squared and K_ν is the modified Bessel function of the second kind of order ν . If the product σv varies slowly with v , an expansion in powers of v^2 holds as

$$\sigma v \simeq a + b v^2, \quad (5)$$

with constant a and b , so that $\langle \sigma v \rangle_{\text{th}} = a + 3bT/(2m_\chi)$. At the lowest order in the non-relativistic expansion, the value of $\langle \sigma_{\text{ann}} v \rangle_{\text{th}}$ is then independent of the WIMP velocity distribution and, if the pre-factor a is a constant, it is the same throughout the history of the Universe.

¹ The title of our paper is inspired by Lacki & Beacom (2010), who also considered constraints on the WIMP parameters.

Near resonances and thresholds where σv varies rapidly with v , such an expansion is no longer valid, and the analysis in Eq. (4) has to be implemented. Co-annihilation can be handled in realistic model thanks to numerical packages (Bringmann et al. 2018; Bélanger et al. 2018). In the following, we assume that the chemical decoupling occurs in the standard cosmology, during the radiation domination period. This assumption can be relaxed to include the production in non-standard cosmological scenarios (Gelmini & Gondolo 2006; Acharya et al. 2009; Visinelli 2018).

Following the methods outlined by Steigman et al. (2012); Baum et al. (2017), we compute the expression for $\langle \sigma v \rangle_{\text{th}}$ that yields a fraction $f_\chi = \Omega_\chi / \Omega_{\text{DM}}$ of WIMPs produced through thermal freeze-out (Lee & Weinberg 1977; Hut 1977; Sato & Kobayashi 1977) at the lowest order in T/m_χ ,

$$\langle \sigma v \rangle_{\text{th}} = \langle \sigma v \rangle_{\text{DM}} f_\chi^{-1.0}, \quad (6)$$

where $\langle \sigma v \rangle_{\text{DM}} = 2.5 \times 10^{-26} \text{ cm}^3 \text{ s}^{-1}$. The expression is valid over a vast range of WIMP masses $m_\chi \gtrsim 10 \text{ GeV}$ and of WIMP density fractions. The deviation from the behaviour $\langle \sigma v \rangle_{\text{th}} \propto f_\chi^{-1}$ expected from Eq. (3) is due to the changes in the relativistic degrees of freedom with temperature.

At temperatures below T_F , the relativistic plasma and WIMPs continue to exchange energy and momentum even if the comoving number of WIMPs is fixed at the value n_{eq} . This condition occurs until the WIMP scattering rate falls below the Hubble rate (Bernstein et al. 1985), after which the scattering process is no longer efficient and WIMPs also decouple *kinetically*. The WIMP kinetic decoupling (KD) occurs at the temperature (Bringmann & Hofmann 2007; Visinelli & Gondolo 2015)

$$T_{\text{KD}} = \frac{m_\chi}{\Gamma(3/4)} \left(\frac{g m_\chi}{M_{\text{Pl}}} \right)^{1/4}, \quad (7)$$

where $g \approx 10.9$ for temperatures in the range 0.1–10 MeV and $\Gamma(3/4) \approx 1.225$. The corresponding Hubble rate and time are H_{KD} and $t_{\text{KD}} = 1/(2 H_{\text{KD}})$, respectively.

3 STRUCTURE OF THE DARK-MATTER HALOS

It is well known that the presence of a massive black hole can lead to a *spike* in the WIMP density profile due to the adiabatic accretion (Gondolo & Silk 1999). Starting from a WIMP cusp with a profile $\propto r^{-\gamma}$, the effect of accreting into a black hole leads to a spike with a profile $r^{-\gamma_{\text{sp}}}$, with $\gamma_{\text{sp}} = (9 - 2\gamma)/(4 - \gamma)$.

However, non-relativistic WIMPs produced after freeze-out can already be gravitationally bound to PBHs at the onset of PBH formation in the early Universe (Ricotti et al. 2008; Lacki & Beacom 2010; Saito & Shirai 2011; Xu et al. 2020). PBHs are formed during the radiation-dominated epoch in the standard cosmology from the direct collapse of mildly non-linear perturbations. After PBH formation, the WIMPs will be gravitationally attracted to the PBHs, leading to the formation of halos. Their form depends on the specific circumstances and particle velocities. The fraction of WIMPs with low velocities remain gravitationally bound to the PBHs and form a density spike around them.

Consider a PBH of mass M forming after WIMP kinetic decoupling. A particle at a distance r from the position

of the PBH would experience the gravitational attraction $\sim GM/r^2$, while at the same time it would be accelerated by the expansion of the Universe at the rate $H^2 r$. Here, we assume that the WIMP kinetic decoupling occurs during radiation domination, when the Hubble rate depends on cosmic time t as $H = 1/(2t)$. The turn-around radius of the WIMP orbit $r_{\text{ta}}(t)$ is found when the gravitational attraction is comparable in magnitude with the Hubble expansion rate. A detailed numerical solution for the turn-around radius obtained from the WIMP equation of motion is well approximated by (Adamek et al. 2019)

$$r_{\text{ta}}(t) \approx [r_S (ct)^2]^{1/3}, \quad (8)$$

where $r_S = 2GM/c^2$ and c is the speed of light. The radius $r_{\text{ta}}(t)$ in Eq. (8) is also the evolving radius within which the cosmological mass is comparable to the PBH mass; overdensities do not grow during the radiation era.

At the time of matter-radiation equality t_{eq} , the WIMP density profile around a PBH of mass M corresponds to a spike with density profile (Adamek et al. 2019)

$$\begin{aligned} \rho_{\chi, \text{spike}}(r) &= f_\chi \frac{\rho_{\text{eq}}}{2} \left(\frac{r_{\text{ta}}(t_{\text{eq}})}{r} \right)^{9/4} \\ &= f_\chi \frac{\rho_{\text{eq}}}{2} \left(\frac{M}{M_\odot} \right)^{3/4} \left(\frac{\bar{r}}{r} \right)^{9/4}, \end{aligned} \quad (9)$$

where $\bar{r} \equiv (2GM_\odot t_{\text{eq}}^2)^{1/3} \approx 0.0193 \text{ pc}$ is the turn-around radius at matter-radiation equality for a PBH of Solar mass and the energy density $\rho_{\text{eq}} = 3H_{\text{eq}}^2 m_{\text{Pl}}^2/(8\pi)$ is defined in terms of the Hubble rate at time t_{eq} , H_{eq} . Equation (9) only applies up to the radius $r_{\text{ta}}(t_{\text{eq}})$ and it is easily seen that the mass within this radius is comparable to M .

The treatment above does not take into account the orbital motion of WIMPs bound to the PBH. We assume that the velocity distribution is described by a function $f(\mathbf{v})$ normalised such that $\int d^3\mathbf{v} f(\mathbf{v}) = 1$. The density of WIMPs orbiting a PBH on bound elliptic orbits is (Eroshenko 2016)

$$\rho_{\chi, \text{tot}}(r) = \frac{2}{r^2} \int d^3\mathbf{v} f(\mathbf{v}) \int_0^{+\infty} dr_i r_i^2 \frac{\rho_i(r_i)}{\tau_{\text{orb}}} \left(\frac{dr}{dt} \right)^{-1}, \quad (10)$$

where the WIMP density profile at PBH formation is $\rho_i(r_i) = \rho_{\text{KD}}$ before kinetic decoupling and matches Eq. (9) after this,

$$\rho_i(r) = \frac{\rho_{\chi, \text{spike}}(r) \rho_{\text{KD}}}{\rho_{\chi, \text{spike}}(r) + \rho_{\text{KD}}}. \quad (11)$$

The orbital period τ_{orb} and the radial speed dr/dt are given in Eqs. (A2a) and (A2b) respectively. In Appendix A we revise the integration over the WIMP phase-space in Eq. (10).

Following the discussion in Adamek et al. (2019), the ratio of the WIMPs' kinetic and potential energies at the turn-around radius is

$$\frac{E_k}{E_p} = \frac{2k_B T_{\text{KD}}}{m_\chi} \frac{ct_{\text{KD}}}{\sqrt{r_S r_{\text{ta}}(t_{\text{KD}})}} = \frac{2k_B T_{\text{KD}}}{m_\chi} \left(\frac{ct_{\text{KD}}}{r_S} \right)^{2/3}, \quad (12)$$

so the kinetic term can be neglected for

$$M \gtrsim 10^{-5} M_\odot (m_\chi/\text{TeV})^{-17/8}. \quad (13)$$

If the kinetic energy distribution can be neglected, Eq. (10)

returns the same distribution as in Eq. (9) times a concentration parameter $\alpha_E \approx 1.53$, as derived using Eq. (A7) in Appendix A.

After matter-radiation equality, the mass gravitationally bound by the PBH grows according to

$$\tilde{M}(z) = M \left(\frac{1 + z_{\text{eq}}}{1 + z} \right). \quad (14)$$

The accretion halts around the epoch of galaxy formation, which we set at $z_* \sim 10$, because of the effects of dynamical friction between DM halos and hierarchical structure formation. At a given redshift, the self-similar secondary infall for the mass accretion and virialisation of DM density spike has the same radial dependence as Eq. (9). This is confirmed by the numerical calculations in Adamek et al. (2019).

The WIMP population inside the halo is consumed by self-annihilation (Berezinsky et al. 1992). We estimate its maximum concentration at redshift z as

$$\rho_{\chi, \text{max}}(z) = f_\chi \frac{m_\chi H(z)}{\langle \sigma v \rangle_H}. \quad (15)$$

Here, $H(z)$ is the Hubble rate at redshift z , while $\langle \sigma v \rangle_H$ is the velocity times the WIMP self-annihilation cross-section in the halo, averaged over the velocity distribution of WIMPs which we assumed to be a Boltzmann distribution with dispersion v_{rms} . For the Taylor expansion in Eq. (5), this average leads to $\langle \sigma v \rangle_H = a + 3b v_{\text{rms}}^2$, so it generally differs from the results for the thermal average $\langle \sigma v \rangle_{\text{th}}$ when higher terms in the expansion are taken into account. In the following, we neglect higher-order terms in the expansion in Eq. (5) and we set $\langle \sigma v \rangle_H = \langle \sigma v \rangle_{\text{th}}$.

The WIMP profile is then

$$\rho_\chi = \frac{\rho_{\chi, \text{tot}}(r) \rho_{\chi, \text{max}}(z)}{\rho_{\chi, \text{tot}}(r) + \rho_{\chi, \text{max}}(z)}, \quad (16)$$

with the plateau region in Eq. (15) that extends to the radius r_{cut} defined implicitly from Eq. (10),

$$\rho_{\chi, \text{tot}}(r_{\text{cut}}) \approx \rho_{\chi, \text{max}}(z). \quad (17)$$

Even if both $\rho_{\chi, \text{tot}}(r)$ and $\rho_{\chi, \text{max}}(z)$ are proportional to the pre-factor f_χ , which cancels out on both sides of Eq. (17), the value of r_{cut} still depends on f_χ through the cross-section $\langle \sigma v \rangle_H$. For example, if the WIMP kinetic energy can be neglected, we obtain

$$\frac{r_{\text{cut}}}{\bar{r}} = \left[\alpha_E \frac{\rho_{\text{eq}}}{2} \left(\frac{M}{M_\odot} \right)^{3/4} \frac{\langle \sigma v \rangle_H}{m_\chi H(z)} \right]^{4/9}. \quad (18)$$

Figure 1 shows the WIMP density profile in Eq. (16) around a PBH of mass M_\odot , for $m_\chi = 10 \text{ GeV}$ (dashed line), $m_\chi = 100 \text{ GeV}$ (solid line), and $m_\chi = 1 \text{ TeV}$ (dotted line). We have fixed $f_\chi = 1$ and $z = 0$. The density profile is characterised by a plateau region in the inner orbits, given by Eq. (15). In the outer region, the profile is described by the solution to Eq. (10).

3.1 WIMP Decay Rate

As we discuss in the previous Section, WIMPs concentrating around an individual black hole are described by a density profile ρ_χ . Their self-annihilation proceeds at the rate

$$\Gamma_0 = \frac{\langle \sigma v \rangle_H}{m_\chi^2} \int dV \rho_\chi^2, \quad (19)$$

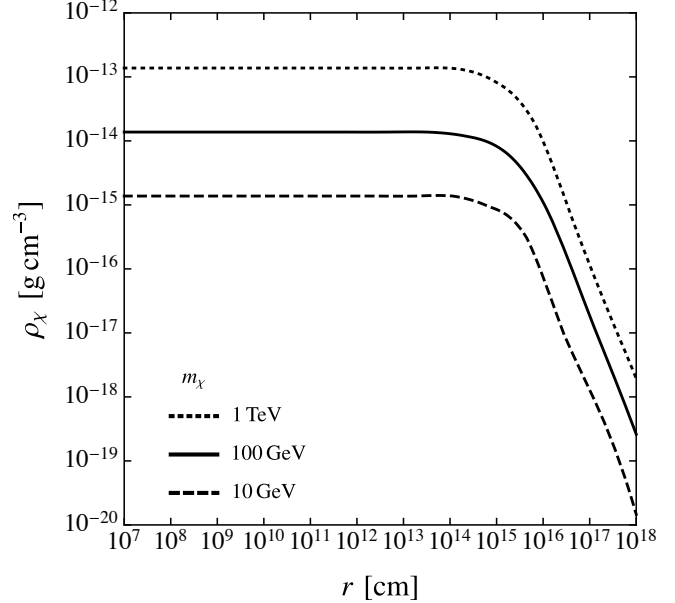


Figure 1. Density profile of WIMPs bound to a solar-mass PBH as a function of the radial distance r . We have fixed $f_\chi \simeq 1$ and $z = 0$ and we set $m_\chi = 10 \text{ GeV}$ (dashed line), $m_\chi = 100 \text{ GeV}$ (solid line), and $m_\chi = 1 \text{ TeV}$ (dotted line).

where the integration is taken over the volume of WIMPs around the black hole. Observationally, each black hole in the Galaxy resembles a decaying particle of mass M and decay rate Γ_0 .

We assume that the WIMP density profile around a PBH is described by Eq. (15) in the inner part but falls off as $r^{-\alpha}$ with $\alpha > 0$ in the outer part. Then the decay rate (19) becomes

$$\Gamma_0 = \frac{4\pi \alpha f_\chi^2 H_0 \rho_{\text{eq}}}{3(2\alpha - 3) m_\chi} \left(\frac{\langle \sigma v \rangle_H \rho_{\text{eq}}}{2 m_\chi H_0} \right)^{3/\alpha - 1} r_{\text{ta}}^3(t_0) \\ = \left[\frac{8\pi G t_0^2 \alpha H_0 \rho_{\text{eq}}}{3(2\alpha - 3) m_\chi} \left(\frac{\langle \sigma v \rangle_{\text{DM}} \rho_{\text{eq}}}{2 m_\chi H_0} \right)^{3/\alpha - 1} \right] M f_\chi^{3-3/\alpha}, \quad (20)$$

where in the last step we have used the expression for $\langle \sigma v \rangle_H$ in Eq. (6) and the definition for $r_{\text{ta}}(t)$ in Eq. (8) at time t_0 . When the WIMP kinetic energy can be neglected, $\alpha = 9/4$ and the decay rate (19) gives

$$\Gamma_0 = \frac{3}{8} \left(\frac{\langle \sigma v \rangle_H \rho_{\text{eq}} H_0^2}{2 m_\chi^4} \right)^{1/3} f_\chi^2 M \equiv \Upsilon f_\chi^{1.7} M, \quad (21)$$

where the quantity Υ has units of $\text{g}^{-1} \text{s}^{-1}$.

4 GAMMA-RAY FLUX FROM WIMP ANNIHILATION

The usual assumption in previous analyses is that WIMPs provide most of the dark matter ($f_\chi \approx 1$), this then implying strong constraints on $f_{\text{PBH}}(M)$. Indeed, we follow this approach in Sections 4.1 to 4.3 below. However, motivated by the claimed evidence for PBHs, we also consider the possibility that PBHs comprise most of the DM, this then placing interesting constraints on f_χ . In the intermediate situation,

in which $f_{\text{PBH}}(M)$ is significant but less than 1, we will conclude that one needs a third DM component.

4.1 Galactic Background Flux

We assume that the distribution of black holes in the Milky Way tracks the distribution of DM in the galactic halo $\rho_{\text{H}}(R)$, scaled by the fraction f_{PBH} , where R is the Galactocentric distance. The expected flux of γ -rays from the annihilation of WIMPs bound to BHs is (Ullio et al. 2002)

$$\Phi_{\gamma, \text{gal}} = \frac{f_{\text{PBH}} \Gamma_0}{M} N_{\gamma} D(b, \ell). \quad (22)$$

Here we have defined the average number of photons resulting from the annihilation processes as

$$N_{\gamma} = N_{\gamma}(m_{\chi}) = \int_{E_{\text{th}}}^{m_{\chi}} dE \frac{dN_{\gamma}}{dE}, \quad (23)$$

where dN_{γ}/dE is the number of γ -rays emitted from annihilations around the black hole per unit time and energy (Cirelli et al. 2010) and E_{th} is the threshold energy for detection. Numerical expressions for the energy spectrum are coded from the package in Cirelli et al. (2011), see also Amoroso et al. (2019). A fit to the numerical solution for different values of m_{χ} implies $N_{\gamma}(m_{\chi}) \approx 18(m_{\chi}/\text{TeV})^{0.3}$.

In Eq. (22), the D factor is the integral over the solid angle and along the line of sight (los) from the position of the Solar system, at a distance $R_{\odot} \approx 8.5$ kpc from the Galactic centre, in a direction with Galactic coordinates (b, ℓ) ,

$$D(b, \ell) = \frac{1}{4\pi} \int d\Omega \int_{\text{los}} ds \rho_{\text{H}}(R). \quad (24)$$

Here the Galactocentric distance $R = R(s, b, \ell)$ is parametrised in terms of the los distance s as

$$R(s, b, \ell) = \sqrt{s^2 + R_{\odot}^2 - 2R_{\odot}s \cos b \cos \ell}. \quad (25)$$

Due to the dependence on the Galactic coordinates b and ℓ , the flux in Eq. (22) depends on the direction of observation. This aspect has been incorporated, for example, by Carr et al. (2016a), who compute the sky map for different values of (b, ℓ) . Here we focus on the direction of the Galactic centre, where we expect the flux to be strongest.

In principle, it is possible to detect γ -ray ‘point’ sources associated with WIMP annihilations around the PBHs, as shown in the detailed analysis of Bertone et al. (2019). Here we consider the γ -ray diffuse background from WIMP annihilations detectable by the Fermi Large Area Telescope (LAT) (Abdo et al. 2010).² The signal can be analysed with a likelihood analysis in which each Fermi-LAT energy bin is compared with the sum of the astrophysical and WIMP annihilation flux, a method used by Ackermann et al. (2015), Di Mauro & Donato (2015), and Ando & Ishiwata (2015). We take the flux sensitivity to be $\Phi_{\text{res}} \approx 10^{-7} \text{ cm}^{-2} \text{ s}^{-1}$, corresponding to the residual component of the Fermi γ -ray flux that could be explained by DM annihilations when other known astrophysical sources are subtracted.

² While Fermi currently offers the best sensitivity for the WIMP mass range studied here, the sensitivities of the Cherenkov Telescope Array (Acharya et al. 2018) and Large High Altitude Air Shower Observatory (Bai et al. 2019) are better suited above the TeV regime.

m_{χ} (GeV)	$f_{\text{PBH}}^{\text{gal}}$	f_{χ}^{gal}	$f_{\text{PBH}}^{\text{eg}}$	f_{χ}^{eg}
10^1	8×10^{-10}	3×10^{-6}	2×10^{-11}	2×10^{-7}
10^2	8×10^{-9}	2×10^{-5}	2×10^{-10}	1×10^{-6}
10^3	8×10^{-8}	5×10^{-5}	2×10^{-9}	5×10^{-6}
10^4	9×10^{-7}	2×10^{-4}	3×10^{-8}	2×10^{-5}

Table 1. Bounds from the Galactic (gal) and extragalactic (eg) γ -ray flux on f_{PBH} when the DM is mainly WIMPs and on f_{χ} when it is mainly PBHs for different WIMP masses.

This is about one order of magnitude larger than the Fermi point-source sensitivity, $\Phi_{\text{Fermi}} = 6 \times 10^{-9} \text{ cm}^{-2} \text{ s}^{-1}$. When the WIMP kinetic energy can be neglected, the decay rate is given by Eq. (21) and the limit $\Phi_{\gamma, \text{gal}} \leq \Phi_{\text{res}}$ gives the bounds in Table 1. For each WIMP mass, the bound on f_{PBH} assumes $f_{\chi} \approx 1$.

The Galactic population of PBHs can be bound from below by requiring that there be at least one of them within the volume of the Milky Way halo (Carr & Sakellariadou 1999). This gives

$$f_{\text{PBH}} \gtrsim \frac{M}{M_{\text{E}}}, \quad (26)$$

where $M_{\text{E}} \approx 10^{12} M_{\odot}$ is the total halo mass. This intersects the upper bound from WIMP annihilations at a mass scale

$$M^{\text{gal}} = M_{\text{E}} \frac{\Phi_{\text{res}}}{\Upsilon N_{\gamma} D(b, \ell)} \approx 8 \times 10^4 M_{\odot} (m_{\chi}/\text{TeV})^{1.0}. \quad (27)$$

The last numerical exponent is derived from the $\Upsilon \propto m_{\chi}^{-4/3}$ dependence and the numerical fit for $N_{\gamma}(m_{\chi})$.

4.2 Extragalactic Background Flux

In order to discuss the extragalactic component, we first need to specify the cosmological model adopted, which is a flat Λ CDM model with a current radiation density $\Omega_{\text{r}} = 7 \times 10^{-5}$, matter density $\Omega_{\text{m}} = 0.31$ and dark energy density $\Omega_{\Lambda} \approx 0.69$ in units of the critical density (Aghanim et al. 2020). We do not include the effects of cosmological curvature, in contrast to other works (Handley 2019; Di Valentino et al. 2019a; Vagnozzi et al. 2020) or the possibility that dark energy evolves with redshift (Poulin et al. 2019; Di Valentino et al. 2019b). The Hubble rate at redshift z is then $H(z) = H_0 h(z)$, where

$$h(z) = \sqrt{\Omega_{\Lambda} + \Omega_{\text{m}}(1+z)^3 + \Omega_{\text{r}}(1+z)^4}. \quad (28)$$

The extragalactic component of γ -rays is produced by the collective annihilations of WIMPs around PBHs at all redshifts (Ullio et al. 2002),

$$\frac{d\Phi_{\gamma}}{dE \, d\Omega} \Big|_{\text{eg}} = \int_0^{\infty} dz \frac{e^{-\tau_{\text{E}}(z, E)}}{8\pi H(z)} \frac{dN_{\gamma}}{dE} \int dM \Gamma(z) \frac{dn_{\text{PBH}}(M)}{dM}, \quad (29)$$

where ‘eg’ indicates extragalactic, n_{PBH} is the number density of PBHs, $\Gamma(z)$ is the WIMP annihilation rate around PBHs, and τ_{E} is the optical depth at redshift z resulting

from (i) photon-matter pair production, (ii) photon-photon scattering, and (iii) photon-photon pair production (Cirelli et al. 2010; Slatyer et al. 2009). The numerical expressions for both the energy spectrum dN_γ/dE and the optical depth are taken from the package in Cirelli et al. (2011).

When the WIMP velocity distribution can be neglected, the z -dependence of the decay rate obtained from Eq. (21) becomes $\Gamma(z) = \Gamma_0 [h(z)]^{2/3}$, where $\Gamma_0 = \Upsilon f_\chi^{1.7} M$. We can then implement the normalisation of the PBH mass function,

$$\int dM M \frac{dn_{\text{PBH}}(M, z)}{dM} \equiv \rho_{\text{PBH}}(z) = f_{\text{PBH}} \rho_{\text{DM}}(z), \quad (30)$$

to integrate over the mass dependence in Eq. (29). Integrating over the energy and angular dependences leads to an expression for the flux,

$$\Phi_{\gamma, \text{eg}} = \frac{f_{\text{PBH}} \Gamma_0}{2M} \frac{\rho_{\text{DM}}}{H_0} \tilde{N}_\gamma(m_\chi), \quad (31)$$

where ρ_{DM} is the present dark matter density and we have defined the average number of photons produced as

$$\tilde{N}_\gamma(m_\chi) \equiv \int_{z_*}^{\infty} dz \int_{E_{\text{th}}}^{m_\chi} dE \frac{dN_\gamma}{dE} \frac{e^{-\tau_{\text{E}}(z, E)}}{[h(z)]^{1/3}}. \quad (32)$$

Comparing the integrated flux with the sensitivity Φ_{res} yields

$$\begin{aligned} f_{\text{PBH}} &\lesssim \frac{2M H_0 \Phi_{\text{res}}}{\rho_{\text{DM}} \Gamma_0 \tilde{N}_\gamma(m_\chi)} \\ &\approx \begin{cases} 8 \times 10^{-13} (m_\chi/\text{GeV})^{1.1} & (M \gtrsim M_*) \\ \left(\frac{m_\chi}{\text{GeV}}\right)^{-3.7} \left(\frac{M}{10^{-10} M_\odot}\right)^{-1.5} & (M \lesssim M_*) \end{cases}, \end{aligned} \quad (33)$$

where the mass M_* is found by matching the last two expressions,

$$M_* \approx 2 \times 10^{-12} M_\odot (m_\chi/\text{TeV})^{-3.2}. \quad (34)$$

The second line in Eq. (33) is obtained by fitting the numerical solutions in the appropriate PBH mass limits, this being independent of M when the kinetic terms of the WIMPs can be neglected (flat) but mass-dependent otherwise (sloped).

The numerical bounds on the PBH and WIMP fractions for the flat part are shown in Table 1. The extragalactic bound is more stringent than the Galactic one, the ratio being

$$\frac{f_{\text{PBH}}^{\text{eg}}}{f_{\text{PBH}}^{\text{gal}}} \sim \left(\frac{N_\gamma(m_\chi)}{\tilde{N}_\gamma(m_\chi)} \right) \left(\frac{H_0 r_\odot \rho_{\text{H}}(r_\odot)}{c \rho_{\text{DM}}} \right) \sim \mathcal{O}(10^{-2}). \quad (35)$$

The extragalactic bound intersects the cosmological incredulity limit (26) at a mass

$$M_{\text{eg}} = \frac{2 \Phi_{\text{res}}}{\alpha_{\text{E}} \Upsilon H_0^2 \tilde{N}_\gamma(m_\chi)} \approx 5 \times 10^{12} M_\odot (m_\chi/\text{TeV})^{1.1}, \quad (36)$$

where we have used the fit of $\tilde{N}_\gamma(m_\chi)$ and set $M_{\text{E}} \approx 3 \times 10^{21} M_\odot$.

4.3 Combined Results

We now include the effect of the initial WIMP velocity distribution in the computation of the density profile, using Eq. (10). This is important for PBH masses smaller than Eq. (13), which corresponds to the intersect of the sloping and flat curves in Fig. 2. Below this mass, Eq. (10) gives the halo profile, whereas the profile before contraction is given

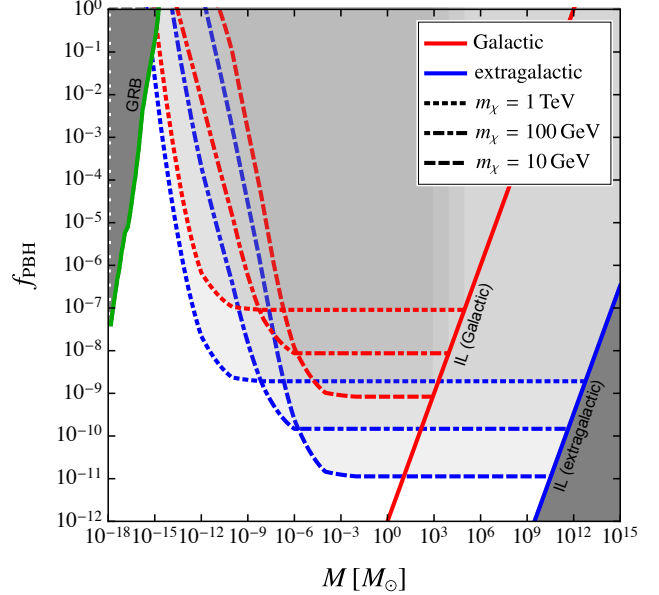


Figure 2. Constraints on f_{PBH} as a function of PBH mass from Galactic (red) or extragalactic (blue) γ -ray background. Results are shown for $m_\chi = 10 \text{ GeV}$ (dashed lines), $m_\chi = 100 \text{ GeV}$ (dot-dashed lines) and $m_\chi = 1 \text{ TeV}$ (dotted lines), setting $\langle \sigma v \rangle = 3 \times 10^{-26} \text{ cm}^3/\text{s}$. Also shown are the Galactic (red solid line) and the extragalactic incredulity limits (blue solid line).

in Eq. (11). The actual WIMP profile at redshift z is then computed from Eq. (16).

The constraints on f_{PBH} if WIMPs provide most of the DM are shown in Fig. 2 for different WIMP masses: $m_\chi = 10 \text{ GeV}$ (dashed lines), $m_\chi = 100 \text{ GeV}$ (solid lines) and $m_\chi = 1 \text{ TeV}$ (dotted lines). The different slopes represent the contributions from the halos formed immediately after DM kinetic decoupling and from later secondary infall around a population of Galactic (red) or extragalactic (blue) PBHs. Our argument cannot place a bound on the PBH fraction above the mass M_{eg} given by Eq. (36).

The flat parts of the constraints correspond to our analysis in Table 1. We note that the sloping parts of the curves in Fig. 2, where the velocity distribution is important, have been derived by Eroshenko (2016) and the flat parts by Adamek et al. (2019). However, this is the first analysis to cover the full PBH mass range. The transition from the sloping to the flat part of the extragalactic limits occurs at approximately the mass M_* given by Eq. (34). The details of the numerical analysis of Eq. (10) are given in Appendix A.

We also show the Galactic bound in Eq. (26) with $M_{\text{E}} = 10^{12} M_\odot$ (red solid line) and the extragalactic bound with $M_{\text{E}} = 3 \times 10^{21} M_\odot$ (blue solid line). Black holes above these bounds are not expected to populate the Galaxy or the Universe. The grey region at the top left of Fig. 2, labelled ‘GRB’, gives the current constraint on f_{PBH} from the soft γ -ray background generated by black hole evaporation (Carr et al. 2010, 2020b; Coogan et al. 2020). It is interesting that WIMP annihilations also give an ‘effective’ black hole decay limit (Adamek et al. 2019), so both limits can be interpreted as being due to decays.

4.4 Constraints on the WIMP population

We now extend the above analysis to the case in which WIMPs do not provide most of the DM. The abundance of thermally-produced WIMPs is set at the onset of their chemical decoupling from the plasma, as discussed in Sec. 2. With the thermal freeze-out mechanism, the WIMP abundance is determined by properties such as the WIMP mass and its interactions with the SM. Although there are currently no bounds on the abundance f_χ in the mass range $m_\chi \gtrsim 1 \text{ GeV}$, this parameter affects the indirect detection of γ -rays from WIMP annihilations (Duda et al. 2002; Baum et al. 2017).

We first modify the above analysis to place a bound on WIMPs if $f_{\text{PBH}} + f_\chi = 1$ but with PBHs providing most of the DM. Since the extragalactic flux (31) is still bound by the sensitivity Φ_{res} , we can proceed as in Sec. 4.2 but considering the solution with $f_\chi \ll f_{\text{PBH}}$. The decay rate is given by Eq. (20) and this leads to

$$f_\chi \lesssim \left(\frac{2M H_0 \Phi_{\text{res}}}{\rho_{\text{DM}} \Gamma_0 \tilde{N}_\gamma(m_\chi)} \right)^{0.6} \quad (37)$$

when the WIMP kinetic energy can be neglected. For different values of the WIMP mass, this gives the bounds shown in Table 1. A numerical fit in this case gives $f_\chi \lesssim 5.5 \times 10^{-5} (m_\chi/\text{TeV})^{0.6}$ and $5 \times 10^{-6} (m_\chi/\text{TeV})^{0.7}$ for the Galactic and extragalactic components, respectively.

Results are shown in Fig. 3 with the values of f_χ indicated by the coloured scale as a function of M (horizontal axis) and m_χ (vertical axis). The colour shows the maximum WIMP DM fraction if most of the DM comprises PBHs of a certain mass and complements the constraints of the PBH DM fraction if most of the DM comprises WIMPs with a certain mass and annihilation cross-section. In this situation, Fig. 2 can also be applied but all the constraints weaken as $f_\chi^{-1.7}$ from Eq. (21).

Clearly, the assumption $f_{\text{PBH}} \approx 1$ used to derive the bound on f_χ cannot be applied for PBH mass ranges in which strong constraints on f_{PBH} can already be placed by other arguments. Indeed, there are only a few mass ranges in which one could have $f_{\text{PBH}} \approx 1$. For example, this is still possible in the range $10^{-15} \text{--} 10^{-10} M_\odot$. In this case, depending on the value of m_χ , the WIMP abundance could vary widely and even be close to 1. However, if PBHs in the mass range $1\text{--}10 M_\odot$ provide most of the DM, as argued by Carr et al. (2019), then one would require $f_\chi \lesssim 10^{-5}$ for all the WIMP masses considered. One could also consider a model with an extended PBH mass function, with a massive population attracting the WIMP halos and a lighter population providing most of the DM. This would still be compatible with the WIMP constraint since the limit on $f_{\text{PBH}}(M)$ is weaker below the mass M_* , given by Eq. (34), and independent of M above this.

The important point is that even a small value of f_{PBH} may imply a strong upper limit on f_χ . For example, if $M_{\text{PBH}} \gtrsim 10^{-11} M_\odot$ and $m_\chi \lesssim 100 \text{ GeV}$, both the WIMP and PBH fractions are $\mathcal{O}(10\%)$. Since neither WIMPs nor PBHs can provide all the DM in this situation, this motivates us to consider situations in which $f_{\text{PBH}} + f_\chi \ll 1$, requiring the existence of a third DM candidate (i.e. the ‘‘something else’’ of our title). Particles which are not produced through the mechanisms discussed above or which avoid annihilation include axion-like particles (Abbott & Sikivie 1983; Dine & Fischler 1983; Preskill et al. 1983), sterile neutrinos (Dodel-

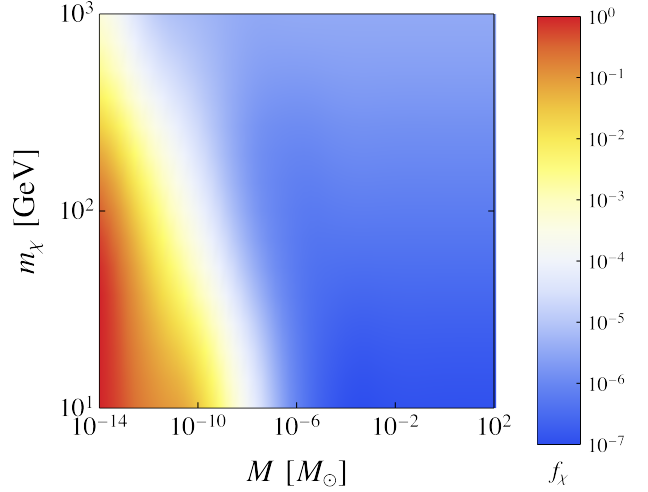


Figure 3. The density plot shows the fraction of WIMPs f_χ (colour bar) as a function of the PBH mass M (horizontal axis) and of the WIMP mass m_χ (vertical axis). We have fixed $f_{\text{PBH}} + f_\chi = 1$.

son & Widrow 1994; Shi & Fuller 1999), ultra-light or ‘‘fuzzy’’ DM (Hu et al. 2000; Schive et al. 2014; Visinelli 2017). Other forms of MACHOs could also serve this purpose.

5 IS SOMETHING ELSE IMPLIED BY PBH DETECTIONS?

We now briefly review several observational hints that PBHs may exist. Each of these observations implies a lower limit on $f_{\text{PBH}}(M)$ for some value of M and the above argument then implies an upper limit on f_χ well below 1. As indicated above, this suggests the existence of a third DM component.

LIGO/Virgo Results — The recent discovery of intermediate mass black hole mergers by the LIGO/Virgo collaboration (Abbott et al. 2020a) might be the first direct detection of PBHs. It is unclear that these gravitational-wave events are primordial in origin. However, if they are, the PBH DM fraction must be larger than 10^{-3} .

Planetary-Mass Microlenses — Using data from the five-year OGLE survey of 2622 microlensing events in the Galactic bulge (Mróz et al. 2017), Niikura et al. (2019) found six ultra-short ones attributable to planetary-mass objects between 10^{-6} and $10^{-4} M_\odot$. These would contribute $\mathcal{O}(1\%)$ of the dark matter.

Pulsar Timing — Recently, NANOGrav has detected a stochastic signal in the time residuals from their 12.5 year pulsar-timing array data (Arzoumanian et al. 2020). Several groups (Kohri & Terada 2020; De Luca et al. 2020; Vaskonen & Veermäe 2020; Domènec & Pi 2020; Bhattacharya et al. 2020) have attributed this to a stochastic background of gravitational waves from planetary-mass PBHs, this being consistent with the short timescale microlensing events found in OGLE data.

Quasar Microlensing — The detection of 24 microlensed quasars by Mediavilla et al. (2017) would allow up to 25% of galactic halos to be PBHs in the mass range 0.05 to $0.45 M_\odot$. The microlensing could also be explained by intervening

stars, but in several cases the stellar region of the lensing galaxy is not aligned with the quasar, which suggests a population of subsolar objects with $f_{\text{PBH}} > 0.01$. A related claim was previously made by [Hawkins \(2006\)](#).

Cosmic Infrared/X-ray Backgrounds — [Kashlinsky et al. \(2005\)](#) and [Kashlinsky \(2016\)](#) have suggested that the spatial coherence of the X-ray and infrared source-subtracted backgrounds could be explained by a significant density of PBHs larger than $\mathcal{O}(1)M_{\odot}$, the Poisson fluctuations in their number density then producing halos earlier than usual. In such halos, a few stars form and emit infrared radiation, while the PBHs emit X-rays due to accretion.

Ultra-Faint Dwarf Galaxies — The non-detection of galaxies smaller than 10–20 parsecs, despite their magnitude being above the detection limit, suggests compact halo objects in the solar-mass range. Moreover, rapid accretion in the densest PBH halos could explain the observed extreme Ultra-Faint Dwarf Galaxies mass-to-light ratios ([Clesse & García-Bellido 2018](#)). Recent *N*-body simulations ([Boldrini et al. 2020](#)) support this suggestion if PBHs in the mass range 25 – $100 M_{\odot}$ provide at least 1% of the dark matter.

If confirmed, any of these claimed signatures would rule out the thermal WIMP model considered here from providing a significant fraction of the DM. However, our analysis has disregarded the possibility that WIMP halos could be dynamically disrupted if PBHs provide most of the DM, as discussed by [Hertzberg et al. \(2020\)](#), and this might modify our conclusion.

6 DISCUSSIONS AND OUTLOOK

In this work, we have examined the bounds on the WIMP and PBH DM fractions from WIMP annihilations around PBHs with masses from 10^{-18} to $10^{15} M_{\odot}$. Our results are summarised in Fig. 2 for the case $f_{\text{PBH}} \lesssim f_{\chi}$ and in Fig. 3 for the case $f_{\chi} \lesssim f_{\text{PBH}}$.

We have first studied the effects of DM annihilation when the dominant DM component is WIMPs from thermal freeze-out. For PBHs larger than a planetary mass, the expression for the extragalactic γ -ray flux in Eq. (29) is independent of M , so the effect of the PBH mass function is unimportant and the maximally-allowed PBH DM fraction is $f_{\text{PBH}} \lesssim 2 \times 10^{-9} (m_{\chi}/\text{TeV})^{1.1}$ for $M \lesssim 5 \times 10^{12} M_{\odot} (m_{\chi}/\text{TeV})^{1.1}$. However, the limit on f_{PBH} is a decreasing function of mass for small M , so one could have a significant density of both WIMPs and PBHs for M in the asteroid mass range.

We also studied the effects of DM annihilations when the dominant DM component is PBHs. This is particularly relevant for the merging intermediate-mass black holes recently discovered by the LIGO/Virgo collaboration ([Abbott et al. 2020b,c](#)). In particular, the collaboration has reported a gravitational-wave signal consistent with a black hole binary with component masses of $85^{+21}_{-14} M_{\odot}$ and $66^{+17}_{-18} M_{\odot}$. It is hard to form black holes from stellar evolution in this range ([Belczynski et al. 2016; Spera & Mapelli 2017](#)), so this could indicate that the components were of primordial origin. The LIGO/Virgo black holes may not provide all the DM but they must provide at least 1% of it. However, Fig. 3

shows that even this would rule out the standard WIMP DM scenario, so this may require a *third* DM component (the ‘something else’ of our title).

Alternatively, the PBHs could have an extended mass function, so that $f_{\text{PBH}} = 1$ even if the LIGO/Virgo black holes have a much smaller density. In this case, the LIGO/Virgo discovery signals a paradigm shift from microscopic to macroscopic DM. If the PBH mass spectrum is dictated by the thermal history of the Universe, this could solve several other cosmic conundra ([Carr et al. 2019](#)).

Our analysis can be improved by dropping some of the assumptions made. (i) We have assumed the WIMP cross-section does not change during the evolution of the Universe but this is not true if a light mediator leads to a Sommerfeld enhancement of the WIMP annihilation ([Arkani-Hamed et al. 2009](#)). (ii) The cross-section has been fixed to the value required at freeze-out with standard cosmology but its value might vary considerably in non-standard cosmologies (eg. with an early period of matter dominance or some other exotic equation of state ([Gelmini & Gondolo 2008](#))). (iii) We have assumed *s*-channel annihilation but the expected signal from annihilations must be reconsidered if the WIMP velocity distribution plays a rôle in the computation of $\langle \sigma v \rangle$ (e.g. if corrections of order $(v/c)^2$ are to be taken into account). Thus our analysis does not cover other important particle DM candidates, such as the sterile neutrino ([Boyarsky et al. 2019](#)) or the QCD axion ([Di Luzio et al. 2020](#)). If exotic particles do form gravitationally bound structures around black holes, they would provide a powerful cosmological test due to their unique imprints.

ACKNOWLEDGEMENTS

We thank Bradley Kavanagh for helpful comments. F.K. acknowledges hospitality and support from the Delta Institute for Theoretical Physics. L.V. acknowledges support from the NWO Physics Vrij Programme “The Hidden Universe of Weakly Interacting Particles” with project number 680.92.18.03 (NWO Vrije Programma), which is (partly) financed by the Dutch Research Council (NWO), as well as support from the European Union’s Horizon 2020 research and innovation programme under the Marie Skłodowska-Curie grant agreement No. 754496 (H2020-MSCA-COFUND-2016 FELLINI).

DATA AVAILABILITY

No new data were generated or analysed in support of this research.

REFERENCES

- Abbott L. F., Sikivie P., 1983, *Phys. Lett.*, B120, 133
- Abbott R., et al., 2020a, *Phys. Rev. Lett.*, 125, 101102
- Abbott R., et al., 2020b, *Phys. Rev. Lett.*, 125, 101102
- Abbott R., et al., 2020c, *Astrophys. J.*, 900, L13
- Abdo A. A., et al., 2010, *Phys. Rev. Lett.*, 104, 101101
- Acharya B. S., Kane G., Watson S., Kumar P., 2009, *Phys. Rev. D*, 80, 083529

Acharya B., et al., 2018, Science with the Cherenkov Telescope Array. WSP ([arXiv:1709.07997](https://arxiv.org/abs/1709.07997)), doi:10.1142/10986

Ackermann M., et al., 2015, *JCAP*, 09, 008

Adamek J., Byrnes C. T., Gosencu M., Hotchkiss S., 2019, *Phys. Rev.*, D100, 023506

Aghanim N., et al., 2020, *A&A*, 641, A6

Amoroso S., Caron S., Jueid A., Ruiz de Austri R., Skands P., 2019, *JCAP*, 05, 007

Ando S., Ishiwata K., 2015, *JCAP*, 05, 024

Arkani-Hamed N., Finkbeiner D. P., Slatyer T. R., Weiner N., 2009, *Phys. Rev. D*, 79, 015014

Arzoumanian Z., et al., 2020, arXiv e-prints, p. [arXiv:2009.04496](https://arxiv.org/abs/2009.04496)

Bai X., et al., 2019, arXiv e-prints, p. [arXiv:1905.02773](https://arxiv.org/abs/1905.02773)

Baum S., Visinelli L., Freese K., Stengel P., 2017, *Phys. Rev. D*, 95, 043007

Bélanger G., Boudjema F., Goudelis A., Pukhov A., Zaldivar B., 2018, *Comput. Phys. Commun.*, 231, 173

Belczynski K., et al., 2016, *Astron. Astrophys.*, 594, A97

Berezhinsky V., Gurevich A., Zybin K., 1992, *Phys. Lett. B*, 294, 221

Bernstein J., Brown L. S., Feinberg G., 1985, *Phys. Rev. D*, 32, 3261

Bertone G., Coogan A. M., Gaggero D., Kavanagh B. J., Weniger C., 2019, *Phys. Rev. D*, 100, 123013

Bhattacharya S., Mohanty S., Parashari P., 2020

Boldrini P., Miki Y., Wagner A. Y., Mohayaee R., Silk J., Arbey A., 2020, *Mon. Not. Roy. Astron. Soc.*, 492, 5218

Boucenna S. M., Kuhnel F., Ohlsson T., Visinelli L., 2018, *JCAP*, 1807, 003

Boyarsky A., Drewes M., Lasserre T., Mertens S., Ruchayskiy O., 2019, *Prog. Part. Nucl. Phys.*, 104, 1

Bringmann T., Hofmann S., 2007, *JCAP*, 04, 016

Bringmann T., Scott P., Akrami Y., 2012, *Phys. Rev. D*, 85, 125027

Bringmann T., Edsjö J., Gondolo P., Ullio P., Bergström L., 2018, *JCAP*, 07, 033

Cai R.-G., Yang X.-Y., Zhou Y.-F., 2020, arXiv e-prints, p. [arXiv:2007.11804](https://arxiv.org/abs/2007.11804)

Carr B. J., Hawking S., 1974, *Mon. Not. Roy. Astron. Soc.*, 168, 399

Carr B., Kühn F., 2020, *Annual Review of Nuclear and Particle Science*, 70, 355

Carr B. J., Sakellariadou M., 1999, *Astrophys. J.*, 516, 195

Carr B. J., Kohri K., Sendouda Y., Yokoyama J., 2010, *Phys. Rev. D*, 81, 104019

Carr B., Kohri K., Sendouda Y., Yokoyama J., 2016a, *Phys. Rev. D*, 94, 044029

Carr B., Kuhnel F., Sandstad M., 2016b, *Phys. Rev. D*, 94, 083504

Carr B., Clesse S., García-Bellido J., Kuhnel F., 2019, arXiv e-prints, p. [arXiv:1906.08217](https://arxiv.org/abs/1906.08217)

Carr B., Kuhnel F., Visinelli L., 2020a, *Mon. Not. Roy. Astron. Soc.*

Carr B., Kohri K., Sendouda Y., Yokoyama J., 2020b, arXiv e-prints, p. [arXiv:2002.12778](https://arxiv.org/abs/2002.12778)

Chapline G., 1975, *Nature (London)*, 253, 251

Cirelli M., Panci P., Serpico P. D., 2010, *Nucl. Phys.*, B840, 284

Cirelli M., et al., 2011, *JCAP*, 1103, 051

Clesse S., García-Bellido J., 2018, *Phys. Dark Univ.*, 22, 137

Coogan A., Morrison L., Profumo S., 2020, arXiv e-prints, p. [arXiv:2010.04797](https://arxiv.org/abs/2010.04797)

De Luca V., Franciolini G., Riotto A., 2020, arXiv e-prints, p. [arXiv:2009.08268](https://arxiv.org/abs/2009.08268)

Di Luzio L., Giannotti M., Nardi E., Visinelli L., 2020, *Phys. Rept.*, 870, 1

Di Mauro M., Donato F., 2015, *Phys. Rev. D*, 91, 123001

Di Valentino E., Melchiorri A., Silk J., 2019a, *Nat. Astron.*, 4, 196

Di Valentino E., Ferreira R. Z., Visinelli L., Danielsson U., 2019b, *Phys. Dark Univ.*, 26, 100385

Dine M., Fischler W., 1983, *Phys. Lett.*, B120, 137

Dodelson S., Widrow L. M., 1994, *Phys. Rev. Lett.*, 72, 17

Domènec G., Pi S., 2020, arXiv e-prints, p. [arXiv:2010.03976](https://arxiv.org/abs/2010.03976)

Duda G., Gelmini G., Gondolo P., 2002, *Phys. Lett. B*, 529, 187

Eroshenko Yu. N., 2016, *Astron. Lett.*, 42, 347

Eroshenko Yu., 2020, *Int. J. Mod. Phys. A*, 35, 2040046

Gelmini G. B., Gondolo P., 2006, *Phys. Rev. D*, 74, 023510

Gelmini G. B., Gondolo P., 2008, *JCAP*, 10, 002

Gondolo P., Gelmini G., 1991, *Nucl. Phys. B*, 360, 145

Gondolo P., Silk J., 1999, *Phys. Rev. Lett.*, 83, 1719

Griest K., Seckel D., 1991, *Phys. Rev. D*, 43, 3191

Handley W., 2019, arXiv e-prints, p. [arXiv:1908.09139](https://arxiv.org/abs/1908.09139)

Hawkins M. R. S., 2006, *Astron. Astrophys.*

Hertzberg M. P., Schiappacasse E. D., Yanagida T. T., 2020, *Phys. Lett. B*, 807, 135566

Hooper D., Goodenough L., 2011, *Phys. Lett. B*, 697, 412

Hu W., Barkana R., Gruzinov A., 2000, *Phys. Rev. Lett.*, 85, 1158

Hut P., 1977, *Phys. Lett. B*, 69, 85

Josan A. S., Green A. M., 2010, *Phys. Rev. D*, 82, 083527

Kashlinsky A., 2016, *Astrophys. J.*, 823, L25

Kashlinsky A., Arendt R. G., Mather J., Moseley S. H., 2005, *Nature*, 438, 45

Kohri K., Terada T., 2020, arXiv e-prints, p. [arXiv:2009.11853](https://arxiv.org/abs/2009.11853)

Lacki B. C., Beacom J. F., 2010, *Astrophys. J.*, 720, L67

Lee B. W., Weinberg S., 1977, *Phys. Rev. Lett.*, 39, 165

Mack K. J., Ostriker J. P., Ricotti M., 2007, *Astrophys. J.*, 665, 1277

Mediavilla E., Jiménez-Vicente J., Muñoz J. A., Vives-Arias H., Calderón-Infante J., 2017, *Astrophys. J.*, 836, L18

Mróz P., et al., 2017, *Nature*, 548, 183

Niikura H., Takada M., Yokoyama S., Sumi T., Masaki S., 2019, *Phys. Rev. D*, 99, 083503

Poulin V., Smith T., Karwal T., Kamionkowski M., 2019, *Phys. Rev. Lett.*, 122, 221301

Preskill J., Wise M. B., Wilczek F., 1983, *Phys. Lett.*, B120, 127

Ricotti M., 2007, *Astrophys. J.*, 662, 53

Ricotti M., Gould A., 2009, *Astrophys. J.*, 707, 979

Ricotti M., Ostriker J. P., Mack K. J., 2008, *Astrophys. J.*, 680, 829

Saito R., Shirai S., 2011, *Phys. Lett. B*, 697, 95

Sato K., Kobayashi M., 1977, *Prog. Theor. Phys.*, 58, 1775

Schive H.-Y., Chiueh T., Broadhurst T., 2014, *Nature Phys.*, 10, 496

Scott P., Sivertsson S., 2009, *Phys. Rev. Lett.*, 103, 211301

Shemmer O., Netzer H., Maiolino R., Oliva E., Croom S., Corbett E., di Fabrizio L., 2004, *Astrophys. J.*, 614, 547

Shi X.-D., Fuller G. M., 1999, *Phys. Rev. Lett.*, 82, 2832

Slatyer T. R., Padmanabhan N., Finkbeiner D. P., 2009, *Phys. Rev. D*, 80, 043526

Spera M., Mapelli M., 2017, *Mon. Not. Roy. Astron. Soc.*, 470, 4739

Steigman G., 1979, *Ann. Rev. Nucl. Part. Sci.*, 29, 313

Steigman G., Dasgupta B., Beacom J. F., 2012, *Phys. Rev. D*, 86, 023506

Ullio P., Zhao H., Kamionkowski M., 2001, *Phys. Rev. D*, 64, 043504

Ullio P., Bergstrom L., Edsjo J., Lacey C. G., 2002, *Phys. Rev. D*, 66, 123502

Vagnozzi S., Di Valentino E., Gariazzo S., Melchiorri A., Mena O., Silk J., 2020, arXiv e-prints, p. [arXiv:2010.02230](https://arxiv.org/abs/2010.02230)

Vaskonen V., Veermäe H., 2020, arXiv e-prints, p. [arXiv:2009.07832](https://arxiv.org/abs/2009.07832)

Visinelli L., 2017, *Phys. Rev. D*, 96, 023013

Visinelli L., 2018, *Symmetry*, 10, 546

Visinelli L., Gondolo P., 2015, *Phys. Rev. D*, 91, 083526

Wagoner R. V., Fowler W. A., Hoyle F., 1967, *Astrophys. J.*, 148, 3

Xu Z., Gong X., Zhang S.-N., 2020, *Phys. Rev. D*, 101, 024029

APPENDIX A: SUDDEN ACCRETION

PBHs that form in the surrounding of a distribution of WIMPs lead to a further concentration of particles around them (Ullio et al. 2001). Assuming the conservation of WIMPs phase-space, the density of WIMPs around a PBH is (Eroshenko 2016)

$$\rho(r) = \frac{2}{r^2} \int d^3\mathbf{v} f(\mathbf{v}) \int_0^{+\infty} dr_i r_i^2 \frac{\rho_i(r_i)}{\tau_{\text{orb}}} \left(\frac{dt}{dr} \right), \quad (\text{A1})$$

where r is the radial distance of the WIMP from the PBH, r_i is the position of the WIMP at kinetic decoupling, and the velocity of the WIMP bound to the PBH in units of the speed of light is \mathbf{v} . The velocity distribution is described by the function $f(\mathbf{v})$, which is normalised so that integration over $d^3\mathbf{v}$ gives unity. For this computation, we normalise all radii to the value $r_g = 2GM$ by setting $x = r/r_g$ and $x_i = r_i/r_g$, and the velocity is in units of the speed of light. Here, $\rho_i(x_i)$ is the density of WIMPs around the PBH at kinetic decoupling and at the rescaled position x_i . We define the orbital period and the radial velocity through energy conservation as

$$\tau_{\text{orb}} = \pi r_g z^{3/2}, \quad (\text{A2a})$$

$$\frac{dr}{dt} = \left[\frac{1}{x} - \frac{1}{z} - \left(\frac{x_i v}{x} \right)^2 (1 - y^2) \right]^{-1/2}, \quad (\text{A2b})$$

where we have set the variable $z \equiv x_i/(1 - x_i v^2)$. We rewrite the integral in Eq. (A1) as (Boucenna et al. 2018)

$$\rho(r) = \frac{4}{x} \int_0^{+\infty} dv v f(v) \int dx_i \frac{x_i \rho_i(x_i)}{z^{3/2}} \int_{-1}^1 \frac{dy}{\sqrt{y^2 - y_m^2}}, \quad (\text{A3})$$

where we have assumed that the velocity dispersion depends only on the absolute value $v \equiv |\mathbf{v}|$ and we have introduced

$$y_m^2 = 1 - \left(\frac{x}{x_i v} \right)^2 \left(\frac{1}{x} - \frac{1}{z} \right) \equiv 1 - \zeta_m^2. \quad (\text{A4})$$

The range of integration over the angular momentum is $|y| \geq y_m$, meaning that we integrate over all possible radii that lie between the apsides of the elliptic orbit. In particular, we have $\zeta_m = 1$ when

$$v^2 = \frac{x}{x_i(x + x_i)}. \quad (\text{A5})$$

We then obtain

$$\rho(r) = \frac{4}{x} \int_0^{+\infty} dv v f(v) \int_0^{1/v^2} dx_i \frac{x_i \rho_i(x_i)}{z^{3/2}} \ln \frac{1 + \zeta_m}{1 - \zeta_m}. \quad (\text{A6})$$

We show for clarity the boundaries of the allowed region of integration over which the integration is performed in Fig. A1. The lines denote *i*) the lower bound $x_i > x/(1 + x v^2)$, or $z > x$; *ii*) the line given by Eq. (A5); *iii*) the upper bound $x_i v^2 < 1$ obtained from demanding that orbits be bound. We perform the integration numerically by dividing the integration region into two sub-regions: $x_i \leq x$ and $x_i > x$. For each sub-region, we slice horizontally the portion shown in Fig. A1 between the allowed bounds. In the case where the kinetic energy can be neglected, is equivalent to taking a

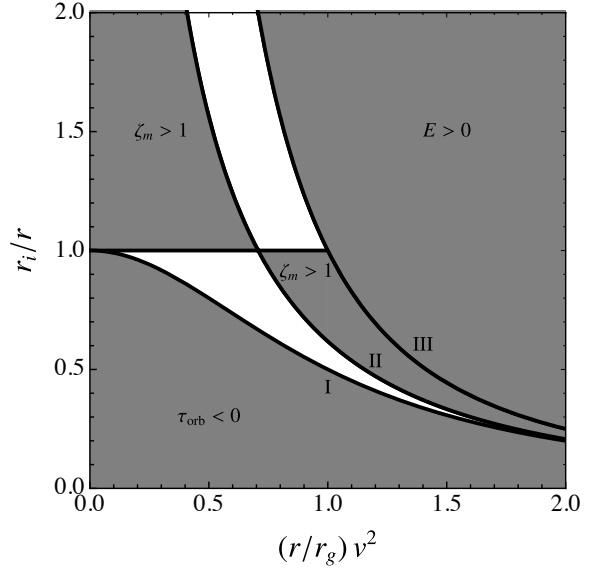


Figure A1. Boundaries of the allowed region of integration for the integral in Eq. (A6). A more detailed description can be found in main text.

delta-function distribution $f(v) \propto \delta(v)$ in Eq. (A1), so that the density of WIMPs around a PBH in this limit reads

$$\rho(r) = \frac{2}{\pi} \int_r^{+\infty} dr_i \frac{r_i}{r^{3/2}} \frac{\rho_i(r_i)}{\sqrt{r_i - r}}, \quad (\text{A7})$$

where $\rho_i(r_i) \equiv \rho_{\text{KD}} (r_M/r_i)^{9/4}$ with $r_M = [r_g (c t_{\text{KD}})^2]^{1/3}$ being the turnaround radius at kinetic decoupling. Performing the integration in Eq. (A7) returns

$$\begin{aligned} \rho(r) &= \frac{2 \rho_{\text{KD}}}{\pi} \left(\frac{r_M}{r} \right)^{9/4} \int_1^{+\infty} d\xi_i \frac{\xi_i^{-5/4}}{\sqrt{\xi_i - 1}} \\ &= \alpha_E \rho_{\text{KD}} \left(\frac{r_M}{r} \right)^{9/4}, \end{aligned} \quad (\text{A8})$$

where $\alpha_E \approx 1.53$. For a power-law profile $\rho(r_i) \propto r_i^{-9/4}$, the procedure then returns the same profile with an additional concentration factor α_E .

This paper has been typeset from a `TeX/LaTeX` file prepared by the author.